New Diamond and Frontier Carbon Technology
Vol. 17, No. 1 2007
MYU Tokyo

NDFCT 530

Scanning Tunneling Microscopy/Spectroscopy on Superconducting Diamond Films

Terukazu Nishizaki*, Yoshihiko Takano[1], Masanori Nagao[1], Tomohiro Takenouchi[2], Hiroshi Kawarada[2] and Norio Kobayashi

Institute for Materials Research, Tohoku University, Sendai 980-8577, Japan
[1]National Institute for Materials Science, 1-2-1 Sengen, Tsukuba 305-0047, Japan
[2]School of Science and Engineering, Waseda University, 3-4-1 Okubo, Shinjyuku-ku, Tokyo 169-8555, Japan

(Received 3 October 2006; accepted 31 October 2006)

Key words: scanning tunneling microscopy/spectroscopy, boron-doped diamond films, superconductivity, energy gap, surface structures

We report on scanning tunneling microscopy/spectroscopy (STM/STS) experiments on (111)-oriented epitaxial films of heavily boron-doped diamond grown by microwave plasma-assisted chemical vapor deposition. STM/STS measurements were performed by ^{3}He-refrigerator-based STM under ultrahigh vacuum. The STM topography on the film surface shows microstructures with a size of ~ 5 – 20 nm and two types of atomic structures: a hydrogenated 1×1 structure, C(111)1×1:H, and an amorphous structure. The tunneling spectra are analyzed by a modified Bardeen, Cooper, and Schrieffer (BCS) expression, and the superconducting energy gap is estimated to be Δ = 0.83 – 0.87 meV at T = 0.47 K. The obtained gap ratio $2\Delta/k_BT_c$ = 3.57 – 3.7 is consistent with the weak-coupling BCS theory. The relatively large value of the broadening parameter Γ ~ 0.38 meV is discussed in terms of the inelastic electron-scattering processes. In the low-temperature region (T = 0.47 K), the tunneling conductance spectra do not show strong spatial dependence, and superconductivity is observed independent of the surface structures. In the high-temperature region (T = 4.2 K), on the other hand, the tunneling conductance spectra show significant spatial dependence, indicating the inhomogeneous distribution of the superconducting property due to the distribution of boron atoms.

1. Introduction

It is known that lightly boron-doped diamond is a *p*-type semiconductor with an activation energy of ~ 0.37 eV. With increasing boron concentration beyond the critical value of $n_c \sim 3\times10^{20}$ cm^{-3} for the metal-insulator (MI) transition, the boron-doped diamond shows metallic behavior. Recently, Ekimov *et al.*[1] have discovered that

*Corresponding author: e-mail: terukazu@imr.tohoku.ac.jp

heavily boron-doped diamond synthesized by a high-pressure high-temperature (HPHT) method shows superconductivity at the transition temperature T_c = 2.3 ~ 4 K. The HPHT diamond used was a polycrystalline bulk sample with a boron concentration of $n \sim 4.9\times10^{21}$ cm^{-3} (i.e., 2.8% of the carbon atoms were substituted by boron).[1] Takano *et al*.[2,3] reported that (111)-oriented polycrystalline boron-doped diamond film shows superconductivity at T_c = 4.2 ~ 7.4 K, which is higher than that reported for HPHT diamond[1] and for boron-doped (001)-oriented single-crystalline diamond films ($T_c \leq$ 2.1 K).[4] By microwave plasma-assisted chemical vapor deposition (MPCVD), a strong carrier-doping dependence of T_c has been reported,[2–5] and the highest T_c reached so far is 7.4 ~ 11.4 K for (111)-oriented epitaxial films with $n \sim 8.4\times10^{21}$ cm^{-3}. [5] According to the doping dependence of T_c,[5] the carrier concentration of the films is considered to be in the underdoped region, and the value of T_c may increase further with increasing carrier density to an optimal value. In addition to the boron concentration n, the value of T_c depends on the process of synthesis and the orientation of the film growth;[5] thus, it is interesting to study the relationship between the surface structure at the atomic scale and the superconducting property.

To understand the electronic structure and the mechanism of the superconductivity in boron-doped diamond, various theoretical proposals[6–10] and experiments[11–14] have been performed. Scanning tunneling microscopy/spectroscopy (STM/STS) is a powerful technique for obtaining high-energy-resolution information about the electron local density of states with subnanometer spatial resolution. Since tunneling spectroscopy provides us with the superconducting gap parameter Δ, the low-energy quasi-particle excitations at the Fermi level, and the electron-phonon coupling strength, the validity of the Bardeen, Cooper, and Schrieffer (BCS) model can be studied for superconductors in the weak and strong limits.

In this paper, we report on low-temperature STM/STS experiments on (111)-oriented epitaxial films of heavily boron-doped diamond. We present two types of atomic structures in the STM topography and the spatial variation of the local density of states in the STS spectra. We discuss the superconducting energy gap structures at different temperatures.

2. Experimental

2.1 *Heavily boron-doped (111) diamond films*

Heavily boron-doped epitaxial diamond films were grown on (111)-oriented type Ib diamond substrates by MPCVD, which is a useful technique for controlling the boron density over a wide range.[2,3,5] Hydrogen, methane, and trimethylboron were used for the source gases. The typical deposition conditions were 800–900ºC substrate temperature, 50 Torr chamber pressure, and 500 W microwave power. Details of the thin-film growth are described elsewhere.[2,3,5] The dc magnetization measurements were performed using a superconducting quantum interface device (SQUID) magnetometer (MPMS-XL), and the superconducting transition temperature was T_c = 5.4 K. The boron concentration was estimated to be $n \sim 6\times10^{21}$ cm^{-3}.[5]

The boron-doped diamond film was annealed at 450ºC in an ultrahigh vacuum (UHV) chamber and was inserted into the cold STM head using a transfer rod without breaking

the vacuum. According to the results of photoemission spectroscopy,[13,14] the annealing procedure was useful for reducing the oxygen/hydrogen contamination at the film surface, because the photoelectron intensity increased after annealing.

2.2 *Scanning tunneling microscopy/spectroscopy*

Using the ^{3}He-refrigerator-based STM (UNISOKU, USM-1300SD2), STM/STS measurements were performed at several temperatures under an UHV (P ~ 10^{-10} Torr) condition. STM/STS can be operated at temperatures as low as ~ 0.47 K on a sample stage when the condensed ^{3}He reaches a base temperature of ≤ 0.3 K. The ^{3}He-refrigerator using a charcoal pump can keep the sample stage at 0.47 K for about 50 h before recondensation is required. A mechanically sharpened Pt-Ir tip approached the boron-doped diamond film perpendicular to the (111) surface. The differential tunneling spectra dI/dV were measured by numerically differentiating the current I – voltage V characteristics and by directly using a lock-in amplifier. The two methods yielded similar results. The typical tunneling parameters for STS measurements were V = 5 – 10 mV and I = 5 – 100 pA for the set sample bias and the current, respectively. The coarse x-y stage of the STM tip, which can be driven by shear piezoelements, was used for macroscopic positioning of the tip over the sample.

3. Results and Discussion

3.1 *Surface structure of heavily boron-doped (111) diamond films*

For the diamond thin film grown by MPCVD, the hydrogen atoms terminate the surface dangling bonds, and this structure is effective in stabilizing the diamond phase during the growth process.[15] The hydrogen-terminated surface is stable under atmospheric conditions, but several atmospheric adsorbates (i.e., H_2O, O_2, CO_2, CH_3, etc.) affect the structural and electronic properties on the hydrogenated surface.[15–17] In order to remove the atmospheric adsorbates, thermal annealing was performed at 450ºC under the UHV condition. After the thermal annealing, we succeeded in making a stable tunneling junction at low temperatures and in obtaining reproducible STM/STS results.

Figure 1 shows the STM topography of the (111)-oriented epitaxial film of heavily boron-doped diamond measured in constant current mode at 4.2 K. The film surface

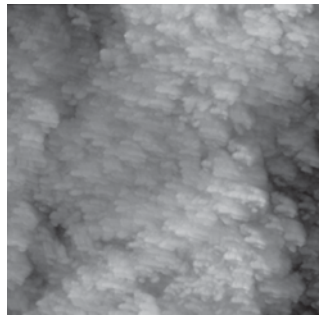

Fig. 1. STM topography of the (111)-oriented epitaxial film of heavily boron-doped diamond at T = 4.2 K (585×585 nm^2, V = 600 mV, I = 0.1 nA).

shows rough structures with a typical size of ~ 1 μm and fine microstructures with a typical size of ~ 5 – 20 nm covering the entire surface of the thin film, as shown above. Recently, similar structures have been reported in single-crystalline thin film of superconducting boron-doped (001) diamond.[18] Since the surface roughness of the heavily boron-doped diamond films is larger than that of the boron-free epitaxial diamond films,[15,19–21] these differences are related to the different growth modes of the heavily boron-doped and the boron-free diamond thin films. As shown in Fig. 1, a flat region is observed within the microstructures; thus, an STM image with an atomic resolution is obtained in the narrow scan area.

On the surface containing the microstructures, the scanning area with the high-quality region is selected by the coarse x-y stage, and a regular atomic arrangement with a sixfold symmetry is observed, as shown in Fig. 2(a). The distance between nearest-neighbor atoms is estimated to be ~ 0.25 nm; the value is in agreement with the distance between the two carbon atoms of the diamond (111) ideal surface. In MPCVD, the density of atomic hydrogen is high; thus, the monohydride structure, C(111)1×1:H, is most likely to be the structure shown in Fig. 2(a). This atomic structure is realized when each dangling bond of diamond (111) 1×1 is terminated by one hydrogen atom, as shown

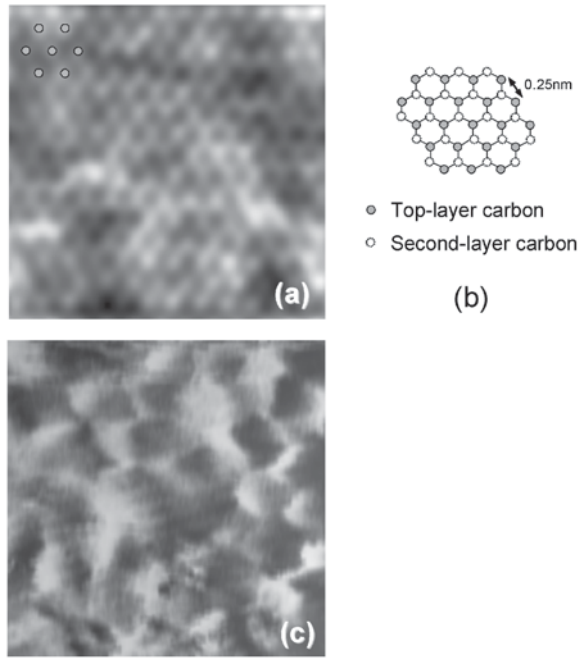

Fig. 2. STM topography of the (111)-oriented epitaxial film of heavily boron-doped diamond at 0.47 K. (a) C(111)1×1:H surface (3.2×3.3 nm^2, V = 500 mV, I = 0.1 nA). (b) Structure of C(111)1×1:H surface. Each dangling bond is terminated by one hydrogen atom. (c) Amorphous region (1.5×1.5 nm^2, V = 600 mV, I = 0.1 nA).

in the structure model of Fig. 2(b). The C(111)1×1:H structure observed in this paper is consistent with previous reports on boron-free diamond (111) films.[15,19,20,22] Although it is difficult to distinguish between carbon and boron atoms in Fig. 2(a) because of the hydrogen termination, the broad change in the background electronic state may result from the random distribution of the doped boron atoms with an estimated concentration of ~3%.[5] In addition, the disorder effect on the atomic arrangement (i.e., atomic distortion, atomic vacancy, etc.) is marked in heavily boron-doped diamond thin film as compared with the boron-free diamond thin films.[15, 19–21]

In a different region on the same film surface, on the other hand, different structures are visible, as shown in Fig. 2(c). The atomic arrangement with a lattice constant of 0.25 ~ 0.35 nm shows a highly disordered (amorphous) structure, which strongly deviates from the hexagonal lattice of the C(111)1×1:H structure. This structure is explained neither by adsorbed hydrocarbons nor by a reconstructed surface. A similar amorphous atomic structure has been observed in the as-grown films of boron-free (100) diamond[23] and has been interpreted as being amorphous carbon.[24] In (111)-oriented epitaxial films of heavily boron-doped diamond, the local high density of boron atoms, the existence of interstitial hydrogen atoms, and the amorphous carbon surface[23,24] are possible origins of the disordered structures. Further development of the surface characterization and STM measurements is necessary to clarify the origin.

3.2 *Superconducting energy gap in heavily boron-doped (111) diamond films*

We performed spectroscopic measurements in several regions: the surface containing the microstructures (Fig. 1), the C(111)1×1:H region (Fig. 2(a)), and the amorphous region (Fig. 2(c)). In the amorphous region, which is observed in the limited area, the tunneling current is less stable, and the superconducting signature in the tunneling spectra is very weak. Except for the amorphous region, almost all regions show stable tunneling spectra, even if the surface contains microstructures. The tunneling spectra in the wide region containing microstructures are essentially the same as those in the C(111)1×1:H region; thus, we discuss the superconducting gap structure in these regions below.

For spectroscopic measurements, the quality of the tunneling junction was checked by measuring the dependence of the tunneling spectra on the distance between the tip and the film surface at the same point. The distance can be controlled by changing the magnitude of the junction resistance R_t. Figure 3 shows a series of tunneling spectra for different values of R_t = 0.1, 0.2, 0.4, 0.6, 0.8, and 1.2 GΩ at 0.47 K. All spectra exhibit the characteristic features of superconductivity, such as a suppression of the tunneling conductance near the zero bias and a coherence peak at ±Δ. These spectra are scaled onto one single curve of the normalized conductance independent of R_t. Therefore, our spectroscopic measurement is performed under the clean vacuum-tunneling condition, and the tip does not perturb the electronic state of the film surface.

In order to study the spatial dependence of the superconducting properties, STS measurements were performed in the wide region. The inset of Fig. 4 shows the topographic image for STS measurements at 0.47 K. The STS data shown in Fig. 4 are taken at the ten points marked in the inset of Fig. 4. The tunneling spectra exhibit a

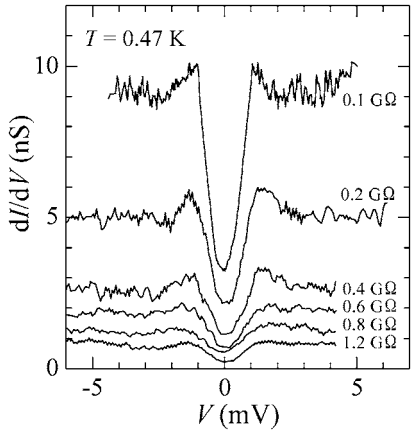

Fig. 3. Differential conductance spectra measured at the same point as a function of tip-sample spacing at 0.47 K. The junction resistance values R_t are 0.1, 0.2, 0.4, 0.6, 0.8, and 1.2 GΩ.

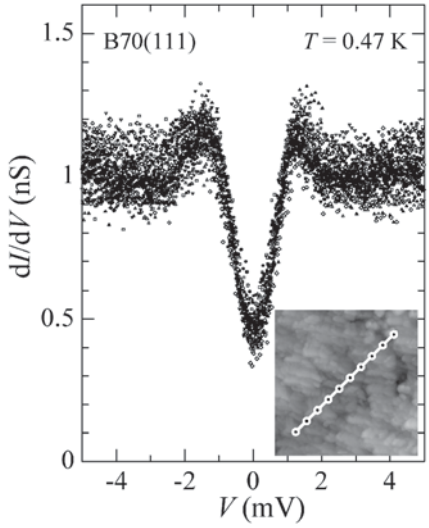

Fig. 4. STS spectra taken at the positions shown in the inset (T = 0.47 K). The spectra at the 10 points are superimposed. Inset: STM topography of (111)-oriented boron-doped diamond film (200 ×200 nm^2, V = 600 mV, I = 0.1 nA).

superconducting energy gap 2Δ, a coherence peak, and symmetric conductance with a metallic background at $V > \Delta$. In addition, the zero-bias conductance shows a relatively high value of about 35% ± 10% of the normal background. This behavior is in contrast with the BCS expression of the density of states without any broadening parameter. These features are reproducible for different tunneling resistances R_t and at different

locations on the film surface in the scanning area of 200×200 nm^2. Since the tunneling conductance spectra are independent of the microstructures, the superconducting order parameter is not changed locally by the microstructures but is homogeneously distributed over a wide range beyond the Ginzburg-Landau coherence length $\xi_{GL} \sim 6.9 - 15$ nm.[1–4]

In the low-temperature region ($T << T_c$), the differential conductance (dI/dV) spectra provide direct information on the local density of states of quasi-particles $N(E, r)$ and consequently on the superconductor gap structure (E: the energy of quasi-particles, r: the position of the STM tip). The tunneling spectrum can be analyzed using the modified BCS expression for the superconducting density of states:[25, 26]

$$N(E,\Gamma) \propto \left| \mathrm{Re} \frac{E - i\Gamma}{\sqrt{(E - i\Gamma)^2 - \Delta^2}} \right|. \quad (1)$$

In the Dynes function, the phenomenological broadening parameter Γ accounts for the pair-breaking effect. Figure 5 shows the experimental tunneling conductance spectrum and the calculated conductance (solid line) using eq. (1). The best fit to the experimental data yields the parameters $\Delta = 0.87$ meV and $\Gamma = 0.38$ meV at $T = 0.47$ K (i.e., $t \equiv T/T_c = 0.087$). Because of the small spatial dependence of the STS spectra, the obtained parameters are distributed within $\Delta = 0.83 - 0.87$ meV and $\Gamma = 0.38 - 0.41$ meV. The value of Δ in this study is consistent with that in recent experiments on the laser-excited photoemission spectroscopy of (111) diamond film ($\Delta = 0.78$ meV at 4 K)[14] and by STM/STS for polycrystalline bulk diamond ($\Delta = 0.8 - 1.0$ meV at 0.5 K).[27] With the measured value of $T_c = 5.4$ K, the gap ratio $2\Delta/k_BT_c = 3.57 - 3.7$ is obtained, and this value is in agreement with the theoretical value $2\Delta/k_BT_c = 3.53$ for a weak-coupling

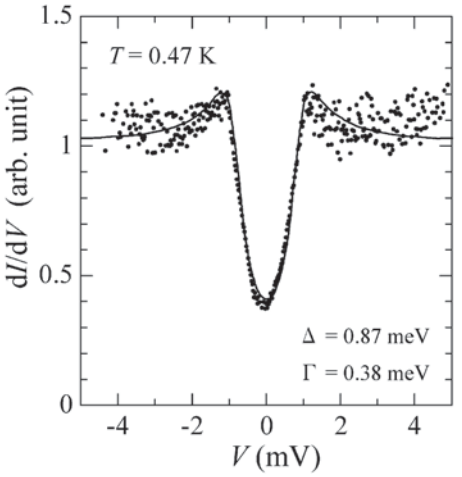

Fig. 5. Typical dI/dV spectrum of (111)-oriented boron-doped diamond film at 0.47 K. The solid line represents the modified BCS density of states (eq. (1)) with the parameters $\Delta = 0.87$ meV and $\Gamma = 0.38$ meV.

BCS superconductor and with STS results for (001)-oriented single-crystalline diamond film.[18] However, the value is much smaller than that of strong-coupling superconductors such as Pb ($2\Delta/k_BT_c = 4.3 - 4.7$)[28] and MgB_2 ($2\Delta/k_BT_c = 4.5$).[29]

The characteristic features of the tunneling spectra observed in this study are the broad coherence peak, the high zero-bias conductance, and the relatively large value of Γ. These results are completely different from recent STM/STS data on (001)-oriented MPCVD diamond film ($T_c = 1.9$ K, $n \sim 1.9\times10^{21}$ cm^{-3}),[18] where the tunneling spectrum is in strong agreement with the weak-coupling BCS expression without the broadening parameter Γ. However, the result of the photoemission experiment on (111)-oriented MPCVD diamond film ($T_c = 7 - 10$ K)[14] is consistent with our results. The large value of Γ cannot be explained in terms of the thermal broadening effect, because our STM/STS experiments were performed at low temperatures ($t = 0.087 << 1$). Consequently, an alternative mechanism of the pair-breaking effect is needed as the origin of the low-energy excitations. Dynes *et al*.[26] suggested that the lifetime broadening of the energy gap edge is due to the inelastic scattering of electrons, and this effect is enhanced in the disordered thin film near the MI transition. The situation may be similar to that of heavily boron-doped diamond films.

Let us discuss a possible origin of the pair-breaking centers in terms of the introduced disorder caused by the boron doping. In this case, the different tunneling spectra of the (001)- and (111)-oriented diamond films can be explained by the different boron concentrations and the different growth modes.[5] With increasing boron concentration, the value of T_c increases because of the carrier doping; however, the introduction of the boron into the diamond produces disorder, which enhances inelastic electron scattering. Umezawa *et al*.[5] pointed out that boron-boron pairs, which distort the diamond lattice locally, are easily formed during (111)-growth rather than (001)-growth. Our STM topography in Fig. 2 also indicates that the disordered structure is marked in the (111)-oriented thin film of the heavily boron-doped diamond as compared with the boron-free diamond film. Considering the intrinsic disorder caused by the heavy boron doping, the characteristic feature of the tunneling spectra with ungapped excitations in the (111)-oriented diamond film can be understood in terms of the inelastic electron scattering. These results indicate that the quasi-particles experience significant scattering, and the pair breaking creates excitations within the gap, which enhance the zero-bias conductance.

Figures 6(a) and 6(b) show the STM topography and the spatial variation of tunneling spectra at the marked positions ($T = 4.2$ K), respectively. In the high-temperature region near T_c, tunneling spectra show a strong spatial dependence, in contrast with the data at $T = 0.47$ K (see Fig. 4). The tunneling spectra in Fig. 6(b) can be classified into three types: weak superconducting gap spectra (positions A to F), normal metallic spectra (positions G and H), and a semiconducting or insulating gap spectrum (position I). These three types of spectra are observed in the whole region measured. The distribution of the tunneling spectra is very small in the low-temperature region ($T << T_c$) but becomes marked in the high-temperature region. The strong spatial dependence of the tunneling spectra at high temperatures can be explained by the local change in the superconducting transition temperature $T_c(r)$, because the measured temperature ($T = 4.2$ K) is slightly below $T_c = 5.4$ K, and the transition width is about $\Delta T_c \sim 1$ K. Since the transition

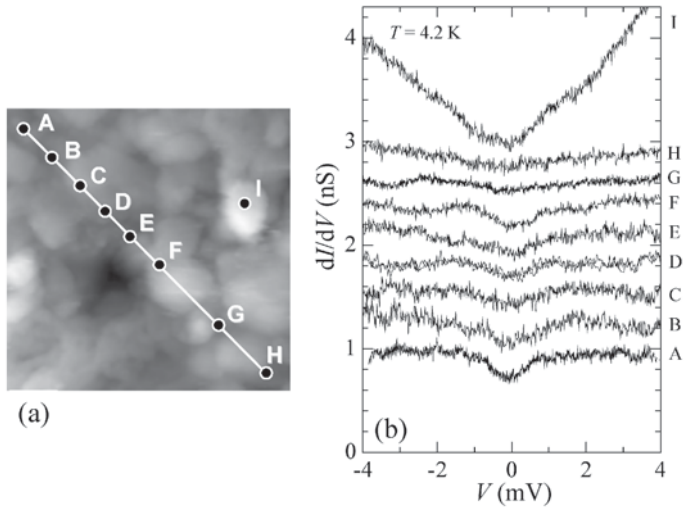

Fig. 6. (a) STM topography of (111)-oriented boron-doped diamond film at 4.2 K (80×80 nm^2, V = 1 V, I = 0.1 nA). (b) STS spectra taken at positions A to I marked in (a). Each subsequent spectrum is offset for clarity.

width tends to increase with increasing boron concentration, the spatial distribution of the tunneling spectra results from the inhomogeneous distribution of boron atoms. On the basis of this scenario, the weak superconducting gap spectra (positions A to F) are observed in the region of $T \leq T_c(r)$ and normal metallic spectra (positions G and H) are observed in the region of $T \geq T_c(r)$. These results indicate that spatially resolved spectroscopic measurement by STM/STS is important for discussing the electronic state and the mechanism of the superconductivity in the heavily boron-doped diamond films with the inhomogeneous property.

4. Summary

We have performed STM/STS experiments on (111)-oriented epitaxial films of heavily boron-doped diamond grown by MPCVD. The STM topography shows microstructures with a size of ~ 5 – 20 nm and two types of atomic structures: a hydrogenated 1×1 structure, C(111)1×1:H, and an amorphous structure. Stable tunneling conductance spectra with superconductivity are observed over a wide region containing both the microstructures and the C(111)1×1:H structures.

In the low-temperature region much below T_c (i.e., t = 0.087), the tunneling conductance spectra do not show spatial dependence, and superconductivity is observed independent of the microstructures. The superconducting energy gap obtained is Δ = 0.83 – 0.87 meV. The corresponding gap ratio $2\Delta/k_BT_c$ = 3.57 – 3.7 is consistent with the theoretical value for weak-coupling BCS superconductors. Considering the intrinsic disorder caused by the heavy boron doping, the characteristic features of the tunneling

spectra, which show a broad coherence peak, a high zero-bias conductance and a large value of Γ, can be explained in terms of the inelastic electron scattering. In the high-temperature region (T = 4.2 K), on the other hand, the tunneling conductance spectra show strong spatial dependence, indicating the inhomogeneous distribution of the superconducting property due to the distribution of boron atoms.

Acknowledgments

The authors acknowledge fruitful discussions with A. Troyanovskiy, T. Sasaki, C. Marcenat and C. Chapelier. This study was partly supported by a Grant-in-Aid for Scientific Research from the Japan Society for the Promotion of Science (JSPS) and the Ministry of Education, Culture, Sports, Science and Technology of Japan (MEXT) and by the CTC program under JSPS.

References

1) E. A. Ekimov, V. A. Sidorov, E. D. Bauer, N. N. Mel'nik, N. J. Curro, J. D. Thompson and S. M. Stishov: Nature **428** (2004) 542.
2) Y. Takano, M. Nagao, I. Sakaguchi, M. Tachiki, T. Hatano, K. Kobayashi, H. Umezawa and H. Kawarada: Appl. Phys. Lett. **85** (2004) 2851.
3) Y. Takano, M. Nagao, T. Takenouchi, H. Umezawa, I. Sakaguchi, M. Tachiki and H. Kawarada: Diamond Relat. Mater. **14** (2005) 1936.
4) E. Bustarret, J. Kačmarčik, C. Marcenat, E. Gheeraert, C. Cytermann, J. Marcus and T. Klein: Phys. Rev. Lett. **93** (2004) 237005-1.
5) H. Umezawa, T. Takenouchi, Y. Takano, K. Kobayashi, M. Nagao, I. Sakaguchi, M. Tachiki, T. Hatano, G. Zhong, M. Tachiki and H. Kawarada: cond-mat/0503303 (2005).
6) G. Baskaran: cond-mat/0404286 (2004).
7) L. Boeri, J. Kortus and O. K. Andersen: Phys. Rev. Lett. **93** (2004) 237002-1.
8) K. W. Lee and W. E. Pickett: Phys. Rev. Lett. **93** (2004) 237003-1.
9) X. Blasé, Ch. Adessi and D. Connétable: Phys. Rev. Lett. **93** (2004) 237004-1.
10) H. J. Xiang, Z. Li, J. Yang, J. G. Hou and Q. Zhu: Phys. Rev. B **70** (2004) 212504-1.
11) V. A. Sidorov, E. A. Ekimov, S. M. Stishov, E. D. Bauer and J. D. Thompson: Phys. Rev. B **71** (2005) 060502-1.
12) J. Nakamura, T. Oguchi, N. Yamada, K. Kuroki, K. Okada, Y. Takano, M. Nagao, I. Sakaguchi, H. Kawarada, R. C. C. Perera and D. L. Ederer: cond-mat/0410144 (2004).
13) T. Yokoya, T. Nakamura, T. Matsushita, T. Muro, Y. Takano, M. Nagao, T. Takenouchi, H. Kawarada and T. Oguchi: Nature **438** (2005) 647.
14) K. Ishizaka, R. Eguchi, T. Tsuda, T. Kiss, T. Shimojima, T. Yokoya, S. Shin, T. Togashi, S. Watanabe, C.-T. Chen, C. Q. Zhang, Y. Takano, M. Nagao, I. Sakaguchi, T. Takenouchi and H. Kawarada: Sci. Tech. Advanced Mater. **7** (2006) 517.
15) H. Kawarada: Surf. Sci. Rep. **26** (1996) 205.
16) J. Ristein, M. Riedel, F. Maier, B. F. Mantel, M. Stammler and L. Ley: J. Phys.: Condens. Matter **13** (2001) 8979.
17) M. Riedel, J. Ristein and L. Ley: Phys. Rev. B **69** (2004) 125338.
18) B. Sacépé, C. Chapelier, C. Marcenat, J. Kačmarčik, T. Klein, M. Bernard and E. Bustarret: Phys. Rev. Lett. **96** (2006) 097006-1.
19) H. Sasaki and H. Kawarada: Jpn. J. Appl. Phys. **32** (1993) L1771.

20) T. Tsuno, T. Tomikawa and S. Shikata: J. Appl. Phys. **75** (1994) 1526.
21) R. E. Stallcup II and J. M. Perez: Appl. Phys. Lett. **81** (2002) 4538.
22) T. Frauenheim, U. Stephan, P. Blaudeck, D. Porezag, H.-G. Busmann, W. Zimmermann-Edling and S. Lauer: Phys. Rev. B **48** (1993) 18189.
23) R. E. Stallcup II, L. M. Villarreal, S. C. Lim, I. Akwani, A. F. Aviles and J. M. Perez: J. Vac. Sci. Technol. B **14** (1996) 929.
24) N. H. Cho, D. K. Veirs, J. W. Ager III, M. D. Rubin and C. B. Hopper: J. Appl. Phys. **71** (1992) 2243.
25) R. C. Dynes, V. Narayanamurti and J. P. Garno: Phys. Rev. Lett. **41** (1978) 1509.
26) R. C. Dynes, J. P. Garno, G. B. Hertel and T. P. Orlando: Phys. Rev. Lett. **53** (1984) 2437.
27) A. Troyanovskiy, T. Nishizaki and E. Ekimov: Sci. Tech. Advanced Mater. **7** (2006) S27.
28) P. Townsend and J. Sutton: Phys. Rev. **128** (1962) 591.
29) F. Giubileo, D. Roditchev, W. Sacks, R. Lamy, D. X. Thanh and J. Klein: Phys. Rev. Lett. **87** (2001) 177008-1.